Available online at www.sciencedirect.com
ScienceDirect
Tetrahedron: Asymmetry
Tetrahedron: *Asymmetry* 17 (2006) 3203–3218

Vibrational circular dichroism DFT study on bicyclo[3.3.0]octane derivatives

Elke Debie,[a] Tom Kuppens,[a] Koen Vandyck,[b] Johan Van der Eycken,[b] Benjamin Van Der Veken,[c] Wouter Herrebout[c] and Patrick Bultinck[a,*]

[a]*Department of Inorganic and Physical Chemistry, Ghent University, Krijgslaan 281-S3, B-9000 Ghent, Belgium*
[b]*Department of Organic Chemistry, Ghent University, Krijgslaan 281-S4, B-9000 Ghent, Belgium*
[c]*Department of Chemistry, University of Antwerp, Groenenborgerlaan 171, B-2020 Antwerp, Belgium*

Received 21 September 2006; accepted 24 November 2006

Abstract—The absolute configurations of four bicylco[3.3.0]octane derivatives: *endo*-bicyclo[3.3.0]octane-2,6-diol, *endo*-2,6-diacetoxybicyclo[3.3.0]octane, *endo*-bicyclo[3.3.0]octane-2,6-dione and bicyclo[3.3.0]octa-2,6-dien-2,6-bistriflate were studied by vibrational circular dichroism (VCD). These chiral derivates are of interest as intermediates in the asymmetric synthesis of enantiomerically pure natural products and chiral ligands for asymmetric catalysis. VCD has been used to determine the absolute configuration of each compound, proving the capability of VCD for molecules with several stereogenic centres. IR and VCD spectra have been simulated at the B3LYP/6-31G* level for all possible diastereomers. Based on the agreement between the experimental and the calculated spectrum, the stereochemistry of each compound could be assigned. The predicted absolute configurations are found to agree with literature data.

1. Introduction

The development of an efficient asymmetric synthesis of the C_2-symmetric *endo*-bicyclo[3.3.0]octane-2,6-diol **1** and bisacetate **2** (Scheme 1)[1] allowed the application of this interesting rigid framework in the asymmetric synthesis of enantiomerically pure natural products, such as the sesquiterpenoids (−)-sulcatine[2] and (+)-kelsoene,[3] prostaglandins,[4,5] the tetramic acid lactam cylindramide,[6] as well as its use in the synthesis of chiral ligands for asymmetric catalysis.[7–9] The racemic ester (±)-**2** can be obtained in one step from commercially available *cyclo*-octa-1,5-diene via Pd^{2+}-catalyzed transannular diacetoxylation, which, after hydrolysis, results in the racemic diol (±)-**1**.[10,1] Initial interest in the biocatalytic resolution of this class of compounds was stimulated by their possible use as intermediates for the synthesis of a prostaglandin synthon. Although this method yielded a high enantiomeric excess for at least one enantiomer, it did not provide an easy and practical method to produce both enantiomers with high enantiomeric excess and yield.[4,11] Nevertheless, *Pseudomonas cepacia* catalyzed kinetic resolution of diol (±)-**1** by transesterification with vinyl acetate in *tert*-butyl methyl ether was later found to provide an easy procedure for the synthesis of larger quantities of both enantiomers of **1** with high enantiomeric excess and yield, making it particulary attractive for application in the synthesis of chiral auxiliaries or ligands.[1]

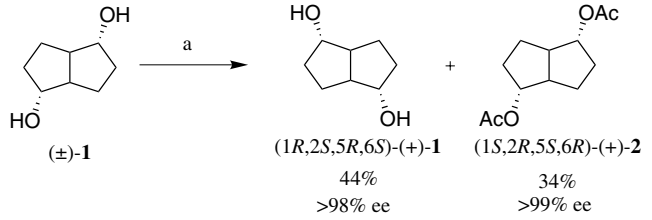

(±)-**1** (1*R*,2*S*,5*R*,6*S*)-(+)-**1** 44% >98% ee (1*S*,2*R*,5*S*,6*R*)-(+)-**2** 34% >99% ee

Scheme 1. Reagents and conditions: (a) vinylacetate, lipase PS, *t*BuOMe, ~22 °C, 240 h.

Lipase catalyzed acylation of (±)-**1** could also be performed with a fluorinated ester, resulting in enantioselective fluorous phase labelling.[12] In most synthetic applications, diol **1** is actually transformed to the C_2-symmetric dione **3** (Scheme 2). This molecule was earlier

* Corresponding author. Tel.: +32 92644423; fax: +32 92644983; e-mail: Patrick.Bultinck@UGent.be

0957-4166/$ - see front matter © 2007 Elsevier Ltd. All rights reserved.
doi:10.1016/j.tetasy.2006.11.046

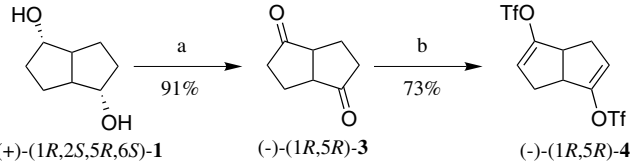

(+)-(1*R*,2*S*,5*R*,6*S*)-**1** (-)-(1*R*,5*R*)-**3** (-)-(1*R*,5*R*)-**4**

Scheme 2. Reagents and conditions: (a) Jones reagent, 1 h, 0 °C, 1 h, rt; (b) (i) KHMDS, −78 °C, 65 min; (ii) $PhNTf_2$, −78 °C, 1 h 55 min; 0 °C, 30 min.

examined by electronical circular dichroism (ECD).[13] In its racemic form, the dione could also be synthesized by alternative methods.[14–16] The absolute configurations of the products obtained were deduced by chemical correlation[4] and used in the determination of the absolute configuration of (−)-sulcatine[2] and (+)-kelsoene[3] as well as in the determination of the stereoselectivity in an enantioselective α-deprotonation–rearrangement of *meso*-epoxides[17] and a transannular cyclization of a chiral *cyclo*-octene derivative.[18]

Herein, the absolute configurations of the enantiomeric series of C_2-symmetric bicyclo[3.3.0]octane compounds **1**, **2**, **3** and **4** (Schemes 1 and 2) were determined by vibrational circular dichroism (VCD). The main advantage of VCD spectroscopy above other techniques to determine absolute configurations is that measurements can be carried out for the molecules in solutions.[19–21] XRD, for example, requires the availability of well-defined crystals and the presence of 'heavy' atoms.[22] In the case of NMR, chiral solvents or chiral shift-reagents are needed to eliminate the degeneracy of the enantiomers.[23] When a chiral molecule does not contain a UV-chromophore, ECD has the disadvantage that it requires extra synthetic steps to introduce chromophores.[24,25] Moreover, calculations of the ECD spectra are more complex than those of VCD spectra. During CD experiments, the differential absorbance of right and left circularly polarized radiation is measured. Considering the VCD, IR light is sent through the sample in order to obtain the vibrational transitions. While enantiomers exhibit the same unpolarized IR spectrum, the bands in the VCD spectra have opposite signs. The spectra thus contain information on the absolute configuration of a molecule through the sign of the bands and can be interpreted, using algorithms for computing VCD intensities,[19,26–28] based on density functional theory (DFT). The absolute configurations of compounds containing only one stereogenic centre are determined on an almost routine basis.[21,29–32] Herein, however, molecules containing more than one stereogenic centre were studied by VCD. Information about the relative configurations of the substituents and the positions of the rings, obtained through other techniques, has not been taken into account. This is analogous to what has been done by Muñoz et al.[33] In other previous VCD studies of molecules, containing more than one chiral centre, the relative configurations of the substituents were always known in advance.[34] In order to determine the absolute configuration, only by using VCD, all optically active diastereomers have to be taken into account. The VCD spectra of each diastereomer then have to be compared with the experiment. In the ideal case, only for one of them could each computed band be linked to a band in the experimental spectrum. All bands of the calculated spectrum of the retained diastereomer either have equal signs with respect to the bands in the experiment or they all are opposite in sign. In the last case, the enantiomer of the diastereomer, for which the VCD calculations were performed, needs to be considered. In this way, the absolute configurations of (+)-**1**, (+)-**2**, (−)-**3** and (−)-**4** have been determined.

2. Results and discussion

2.1. Synthesis

Diol (±)-**1**, obtained by Pd^{2+}-catalyzed transannular diacetoxylation of cycloocta-1,5-diene and subsequent hydrolysis as mentioned above,[1,10] was subjected to lipase catalyzed kinetic resolution resulting in the enantiomerically pure diol (+)-**1** and diacetate (+)-**2** on a multigram scale (∼8–9 g of both (+)-**1** and (+)-**2**) (Scheme 1).[1] The diol was further transformed to dione (−)-**3** by oxidation with Jones reagent (Scheme 2). Dienolization with KHMDS, followed by treatment with $PhNTf_2$, resulted in the formation of the crystalline bisvinylic triflate (−)-**4**. Vinyltriflates, as diene **4**, can serve as interesting intermediates for further synthetic application.[35,36]

2.2. Conformational analysis

2.2.1. Bicyclo[3.3.0]octane-2,6-diol 1. Compound **1** has four stereogenic centres, leading to 16 possible stereoisomers, from which only 12 are symmetry unique. The combinations containing an inversion centre [(1*R*,2*R*,5*S*,6*S*)-**1**, (1*R*,2*S*,5*S*,6*R*)-**1**, (1*S*,2*S*,5*R*,6*R*)-**1** and (1*S*,2*R*,5*R*,6*S*)-**1**] can be omitted, since they are not optically active. The number of diastereomers, under investigation, is therefore limited to four: (1*R*,2*R*,5*S*,6*R*)-**1** = *RRSR*, (1*R*,2*S*,5*R*,6*R*)-**1** = *RSRR*, (1*R*,2*S*,5*R*,6*S*)-**1** = *RSRS* and (1*R*,2*R*,5*R*,6*R*)-**1** = *RRRR*. The first configuration is a *trans*-coupled bicyclic system, whereas the other configurations are *cis*-coupled.

The conformational space of each of the four configurations can be described by means of the orientation of the OH-groups, denoted by τ_1 and τ_2, and the CO torsions, denoted by τ_3 and τ_4. These are shown in Figure 1. The positions of the substituents can be considered as equatorial or axial with respect to the five-membered rings. Three typical minima in the CO torsion potential energy are observed, that is, dihedral angles around 60°, 180° and −60°. These are denoted as G (*gauche* clockwise), T (*trans*) and G′ (*gauche* counterclockwise), respectively. In the conformational notation, the group-ring orientation ('e' or 'a') and the CO torsions (G, T or T′) are given successively for both exocyclic substituents.

A conformational study, described in more detail in Section 4.4, of the first diastereomer, *RRSR*, leads to nine relevant conformations. It was observed that the substituent attached to C6 is always positioned axial, whereas the other is positioned equatorial. For the three most stable conformations, the CO bond torsion of the axial substituent is

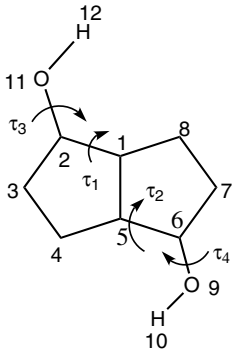

Figure 1. Conformational analysis of **1** through the variation of four torsions: $\tau_1 = O11–C2–C1–C5$, $\tau_2 = O9–C6–C5–C1$, $\tau_3 = H12–O11–C2–C1$ and $\tau_4 = H10–O9–C6–C5$.

180° while the analogous bond torsion of the equatorial substituent varies over the three conformations. The second diastereomer, *RSRR*, has 36 significant conformations. This number can be rationalized because both substituents can either be equatorial or axial. This leads to 4 times the number of conformations of the previous diastereomer (*RRSR*). In Table 1 it can be seen that the energy difference is very small. Due to the lack of symmetry, for both diastereomers, the substituents are distinguishable. In the analysis of the third diastereomer, *RSRS*, only two relevant conformations were found. Both are stabilized by the H–O···H bond interaction, formed between the hydroxy substituents. Due to the C_2-symmetry of this configuration, both substituents are indistinguishable. The global minimum can thus be written as aTaG or aGaT. For the fourth diastereomer, *RRRR*, 11 significant conformations have been found. The two least stable conformations (eGeG and aG′aG′) have a C_2-symmetry. Table 1 shows the labels of the different conformations of each diastereomer together with their corresponding dihedral angles. For each conformation, the Boltzmann populations have been calculated based on their Gibbs free energy differences.

2.2.2. 2,6-Diacetoxybicyclo[3.3.0]octane 2. Although **2** contains four stereogenic centres, again only four diastereomers need to be investigated: (1*R*,2*R*,5*S*,6*R*)-**2** = *RRSR*, (1*S*,2*R*,5*S*,6*S*)-**2** = *SRSS*, (1*S*,2*R*,5*S*,6*R*)-**2** = *SRSR* and

Table 1. B3LYP/6-31G* relative free energies (ΔG^0, in kcal/mol), Boltzmann populations (%*F*, $T = 298.15$ K) and dihedral angles (τ_1, τ_2, τ_3 and τ_4) for the localized conformations of each diastereomer of **1**

	Notation	τ_1	τ_2	τ_3	τ_4	ΔG^0	%*F*
RRSR							
1	eG/aT	−141	65	−103	178	0.00	22.43
2	eG′/aT	−146	−55	−103	−179	0.06	20.40
3	eT/aT	−138	179	−103	179	0.21	15.79
4	eG′/aG′	−147	−58	−97	−62	0.46	10.39
5	eG/aG′	−143	66	−97	−62	0.59	8.35
6	eT/aG′	−140	−179	−97	−61	0.63	7.80
7	eT/aG	−140	−179	−106	55	0.80	5.85
8	eG/aG	−144	69	−106	57	0.83	5.50
9	eG′/aG	−148	−62	−106	54	1.10	3.50
RSRR							
1	aT/aG′	−76	−174	79	−65	0.00	9.98
2	aT/aT	−77	−172	76	176	0.05	9.16
3	aG/aG′	−80	59	79	−64	0.06	9.06
4	aG/aT	−81	60	76	177	0.33	5.67
5	eT/aT	−161	178	73	172	0.52	4.12
6	eG′/aT	−168	−62	73	171	0.59	3.70
7	eT/eG′	−160	176	163	−65	0.63	3.45
8	eG′/eG′	−168	−62	163	−66	0.67	3.21
9	eG/aT	−164	67	73	173	0.67	3.20
10	aT/eG′	−74	−172	165	−65	0.72	2.95
11	eG/eG′	−163	66	163	−64	0.72	2.95
12	eG/aG′	−164	67	77	−71	0.75	2.84
13	aG′/aT	−84	−62	76	176	0.75	2.81
14	eT/aG′	−161	176	77	−73	0.76	2.78
15	aG/eG′	−78	60	165	−64	0.81	2.52
16	eT/eT	−160	178	161	−179	0.88	2.26
17	aG′/aG′	−84	−58	79	−67	0.88	2.25
18	eG′/eG	−167	−61	168	65	0.90	2.20
19	eG′/eT	−167	−63	161	−179	0.92	2.12
20	eG′/aG′	−168	−59	77	−72	0.93	2.06
21	eT/eG	−160	177	168	64	0.96	1.98
22	aT/aG	−76	−173	84	70	0.96	1.98
23	eG/eG	−162	65	168	63	1.09	1.59
24	aG/aG	−80	59	85	66	1.11	1.52
25	eG/eT	−163	66	162	−179	1.13	1.47

(*continued on next page*)

Table 1 (*continued*)

	Notation	τ_1	τ_2	τ_3	τ_4	ΔG^0	%*F*
26	eG′/aG	−168	−62	81	68	1.14	1.46
27	eT/aG	−162	−179	80	66	1.14	1.45
28	aT/eG	−74	−173	168	70	1.15	1.43
29	aG/eG	−78	59	169	68	1.20	1.31
30	aT/eT	−75	−171	162	−178	1.21	1.29
31	aG′/eG′	−82	−60	165	−67	1.23	1.26
32	aG/eT	−78	59	162	−179	1.33	1.07
33	eG/aG	−165	63	81	62	1.40	0.95
34	aG′/aG	−84	−59	84	71	1.54	0.74
35	aG′/eT	−82	−61	162	−179	1.57	0.71
36	aG′/eG	−82	−56	168	73	1.72	0.55
RSRS							
1 *a*	aTaG	75	166	81	47	0.00	69.61
2 *b*	aG′aG	78	−76	81	40	0.50	29.98
RRRR							
1	eGaT	−163	63	−76	−174	0.00	19.01
2	eGaG	−163	64	−80	59	0.00	18.97
3	aGeT	−80	58	−160	176	0.09	16.37
4	aGaT	−78	57	−74	−174	0.34	10.79
5	eG′aG′	−168	−61	−84	−59	0.56	7.36
6	eG′eT	−168	−61	−161	179	0.60	6.94
7	eGaG′	−163	66	−83	−56	0.72	5.65
8	eGeT	−164	65	−161	178	0.80	4.94
9	aG′aT	−82	−54	−74	−173	1.00	3.50
10	aGaG′	−78	60	−82	−56	1.04	3.30
11 (C_2)	eGeG	−164	65	−164	65	1.19	2.55
12 (C_2)	aG′aG′	−82	−58	−82	−58	2.03	0.62

The labels *a* and *b*, found in the first column, are used later on to assign the experimental spectra. The '/' indicates that the labels of each substituent are distinguishable. In cases of symmetry the point group is given in brackets.

(1*S*,2*S*,5*S*,6*S*)-**2** = *SSSS*. The first configuration is a *trans*-coupled bicyclic system, whereas the other configurations are *cis*-coupled. For each of these diastereomers, a conformational analysis has been performed. The conformational space can be described by means of the orientation of the acetate groups; besides the group-ring orientation (τ_1 and τ_4), for each substituent, two dihedral angles need to be taken into account: τ_2 (and τ_5) and τ_3 (and τ_6), as shown in Figure 2.

During conformational analysis of the first configuration, *RRSR*, 46 minima have been found. Based on the energies, only four of them are significant. These conformers have two things in common. While one substituent has an equatorial group-ring orientation, the other substituent is in axial position with respect to the five-membered rings. Secondly, in all cases τ_3 and τ_6 were found to be 180°. These two features give rise to the most stable conformers. Analysis of the second diastereomer, *SRSS*, leads to 135 different minima. Much more combinations are possible because the group-ring orientations of both substituents are not restricted, opposite to the previous configuration. For the most stable conformers, relevant for the construction of the spectra, τ_3 and τ_6 are equal to 180°. Conformational analysis of the third configuration, *SRSR*, also yields 78 minima. In the third configuration, both substituents have the same chirality and are, therefore, indistinguishable. For some of the conformers, the rotational symmetry number is equal to 2. This should be taken into account during the calculations of the Boltzmann populations, using their Gibbs free energies. Only 10 conformers are significant and will be used for the construction of the spectra. For each of them, τ_3 and τ_6 are equal to 180°. Conformational analysis of the last configuration, *SSSS*, is comparable to that of the third one. The substituents are again

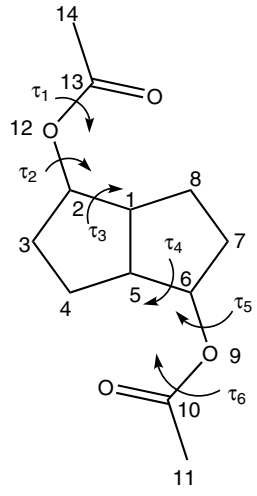

Figure 2. Conformational analysis of **2** through the variation of six torsions: τ_1 = O12–C2–C1–C5, τ_2 = C13–O12–C2–C1, τ_3 = C14–C13–O12–C2, τ_4 = O9–C6–C5–C1, τ_5 = C10–O9–C6–C5 and τ_6 = C11–C10–O9–C6.

Table 2. B3LYP/6-31G* relative free energies (ΔG^0, in kcal/mol) and Boltzmann populations (%F, $T = 298.15$ K) for the localized conformations of each diastereomer of **2**

	τ_1	τ_2	τ_3	τ_4	τ_5	τ_6	ΔG^0	%F
RRSR								
1	155	84	179	78	95	178	0.00	40.40
2	159	165	−179	80	165	179	0.31	24.14
3	156	84	179	79	163	−179	0.43	19.45
4	159	165	−179	79	93	179	0.55	16.01
SRSS								
1	146	78	178	−142	−93	−178	0.00	17.01
2	149	158	−179	−147	−159	180	0.22	11.69
3	145	78	179	−148	−159	180	0.44	8.05
4	91	104	178	−93	−82	−179	0.46	7.77
5	82	161	−180	−156	−160	179	0.49	7.47
6	82	162	179	−153	−95	−179	0.52	7.12
7	150	159	−180	−141	−93	−178	0.53	6.95
8	92	105	178	−94	−161	180	0.57	6.54
9	93	159	−180	−94	−161	180	0.58	6.44
10	93	158	−180	−92	−82	−179	0.69	5.29
11	158	159	−179	−82	−84	−179	0.84	4.14
12	92	99	177	−142	−85	−179	0.88	3.82
13	154	82	179	−84	−162	179	0.89	3.80
14	155	82	179	−81	−84	−180	1.16	2.39
15	157	159	−179	−85	−161	179	1.43	1.52
SRSR								
1 *a*	145	77	179	95	160	−180	0.00	20.28
2 *b*	145	78	179	92	103	178	0.13	16.30
3 *c*	148	159	−180	94	158	−180	0.22	13.93
4 *d*(C_2)	155	82	179	155	82	179	0.26	13.17
5	155	81	178	158	159	−179	0.38	10.66
6	92	103	178	148	158	−179	0.42	9.92
7	91	159	−179	89	99	178	0.60	7.39
8 (C_2)	90	160	−179	90	160	−179	0.76	5.65
9 (C_2)	159	158	−179	159	158	−179	1.53	1.54
10 (C_2)	95	95	178	95	95	178	1.69	1.16
SSSS								
1	−91	−82	−179	−144	−95	−178	0.00	35.91
2	−147	−159	180	−91	−82	−179	0.64	12.25
3	−93	−161	−180	−142	−95	−179	0.67	11.65
4	−93	−161	180	−146	−160	180	0.34	20.38
5 (C_2)	−82	−85	−180	−82	−85	−180	1.73	1.93
6 (C_2)	−139	−82	−179	−139	−82	−179	1.00	6.60
7	−85	−161	179	−82	−84	−179	1.29	4.07
8 (C_2)	−84	−162	180	−84	−162	180	2.10	1.03
9	−145	−159	180	−140	−84	−178	1.37	3.55
10 (C_2)	−148	−161	179	−148	−161	179	1.60	2.41
11	−154	63	180	−90	−83	−180	3.81	0.06
12	−90	−83	−180	−154	63	180	3.76	0.06
13	−93	−161	179	−155	63	180	3.70	0.07
14	−140	−83	−179	−153	62	179	4.43	0.02

For the substituents, the torsions (τ_1, τ_2, τ_3, τ_4, τ_5 and τ_6 in degrees) are given. In case of symmetry, the point group is written between brackets. The labels *a*, *b*, *c* and *d*, found in the first column, are used later on to assign the experimental spectra.

indistinguishable, because they have the same chirality. Again, for some of the conformers a twofold rotation axis can be found. In Table 2, the conformers of each configuration are given together with their Boltzmann populations and the dihedral angles of each substituent.

2.2.3. Bicyclo[3.3.0]octane-2,6-dion 3. This molecule has two stereogenic centres. The *trans*-coupled bicyclic system contains an inversion centre and is optically inactive. Therefore, only one diastereomer has to be taken into account to predict the absolute configuration. Calculations of (1*R*,5*R*)-**3** = *RR* have been performed. During conformational analysis, as described in Section 4.4, two different conformers were found. Their difference in free energy is 1.99 kcal/mol. This leads to populations of 96.6% and 3.3%.

2.2.4. Bicyclo[3.3.0]octa-2,6-dien-2,6-bistriflate 4. For the same reasons as for **3**, only one diastereomer has to be taken into account. Calculations have been performed for (1*R*,5*R*)-**1** = *RR*. During conformational analysis, four

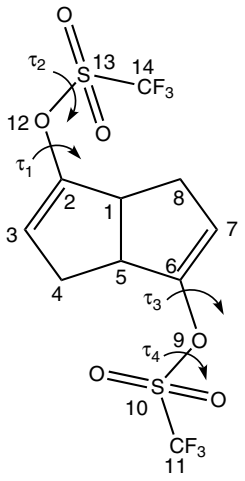

Figure 3. Conformational analysis of **4** through the variation of four torsions: $\tau_1 = S13–O12–C2–C1$, $\tau_2 = C14–S13–O12–C2$, $\tau_3 = S10–O9–C6–C5$ and $\tau_4 = C11–S10–O9–C6$.

dihedrals have been varied, two of each substituent, as shown in Figure 3. The substituents were indistinguishable. In Table 3, the Boltzmann populations of each conformer together with their dihedral angles are shown. Some of the minima contain a twofold rotation axis.

2.3. IR and VCD spectra

In order to determine the absolute configuration of (+)-**1**, eight stereo-isomers have to be considered. It is, however, sufficient to perform calculations for the selected diastereomers: *RRSR*, *RSRR*, *RRRR* and *RSRS*. In Figures 4 and 5, their Boltzmann weighted IR and VCD spectra, respectively, are given. One by one they were compared to the corresponding experimental spectra. By only considering the unpolarized IR spectra, it was very difficult to draw a conclusion about the relative configuration. In the VCD spectrum, however, bands with opposite sign are resolved. This gives extra information during the assignment. The diastereomer with a configuration of *RSRS* seems to show the greatest resemblance with the experiment.

This, however, is not sufficient to reach a conclusion on the absolute configuration of (+)-**1**. In order to gain certainty, it is necessary to perform an assignment of the experimental bands, based on the theoretical spectra of the *RSRS* configuration, calculated at the B3LYP/6-31G* level. This is shown in Figures 6 and 7. Fundamentals designated as *a* originate from conformation aTaG; those designated as *b* represent aG′aG. No label was used when fundamentals of both conformations coincide or have a small difference in frequency. The similarity with the experimental spectrum was found to be much greater than for any of the other possible diastereomers, allowing us to establish the absolute configuration. However, there are also several bands that do not agree completely between experiment and theory. First of all, several bands are not completely resolved. In the experimental IR spectrum, fundamental 19 appears to be a shoulder of fundamental 20, while in the calculated spectra there are two separate bands visible. Fundamentals 26/27 and 31/32 were not resolved in the

Table 3. B3LYP/6-31G* relative free energies (ΔG^0, in kcal/mol) and Boltzmann populations (%*F*, $T = 298.15$ K) for the localized conformations of **4**

RR	C2,C1,O9,S17	C1,O9,S17,C20	C3,C7,O8,S10	C7,O8,S10,C13	ΔG^0	%*F*
1	−82	−103	−122	89	0.000	9.31
2	−81	−102	−68	−163	0.009	9.17
3	−101	167	148	−85	0.103	7.82
4	−81	−101	−98	164	0.155	7.16
5	−82	109	−80	−101	0.158	7.13
6	−97	164	−97	164	0.160	7.10
7	125	−178	−100	168	0.220	6.42
8 (*C*2)	−82	−102	−82	−102	0.278	5.82
9	−83	110	−103	165	0.421	4.57
10	−123	89	−82	110	0.548	3.69
11 (*C*2)	−121	91	−122	90	0.558	3.63
12	125	−179	−122	90	0.574	3.53
13	125	180	−81	−103	0.579	3.51
14	126	−179	−82	111	0.581	3.49
15	149	−85	−82	−103	0.649	3.11
16 (*C*2)	126	−180	126	−180	0.866	2.16
17	−82	−102	105	105	0.868	2.15
18	110	110	150	−83	0.990	1.75
19	104	105	−121	88	1.143	1.35
20	−84	108	148	−84	1.202	1.22
21	148	−85	−102	163	1.349	0.96
22	−122	90	149	−84	1.397	0.88
23 (*C*2)	147	−80	147	−80	1.441	0.82
24	125	−180	150	−82	1.444	0.81
25	105	105	−82	110	1.480	0.77
26 (*C*2)	148	−80	148	−80	1.546	0.69
27	125	180	104	106	1.637	0.59
28 (*C*2)	104	105	104	105	1.872	0.40

The torsions (τ_1, τ_2, τ_3 and τ_4) of each substituent are written in degrees. In cases of symmetry the point group is given in brackets.

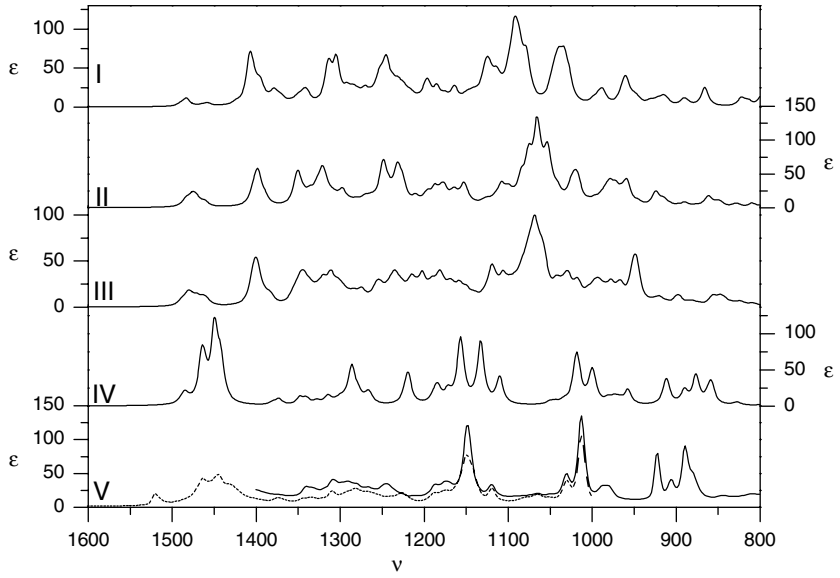

Figure 4. B3LYP/6-31G* IR spectra of each diastereomer of **1**: I—*RRSR*, II—*RRRR*, III—*RSRR*, IV—*RSRS*. Experimental unpolarized IR absorption spectrum of (+)-**1** (V) in CS_2 (solid line, 800–1400 cm^{-1}) and in $CDCl_3$ (dotted line, 1000–1600 cm^{-1}). Experimental and theoretical intensities in L mol^{-1} cm^{-1}; frequencies in cm^{-1}.

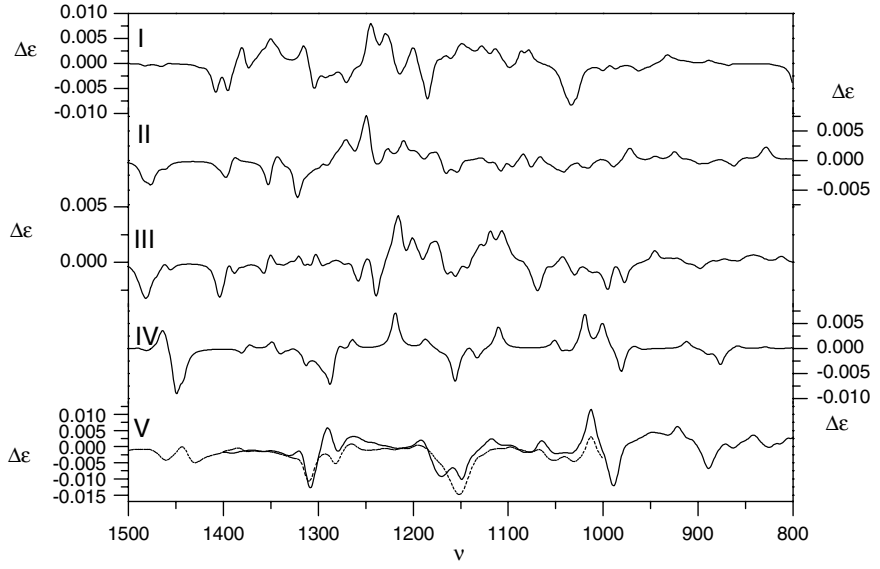

Figure 5. B3LYP/6-31G* VCD spectra of each diastereomer of **1**: I—*RRSR*, II—*RRRR*, III—*RSRR*, IV—*RSRS*. Experimental VCD spectrum of (+)-**1** (V) in CS_2 (solid line, 800–1400 cm^{-1}) and in $CDCl_3$ (dotted line, 1000–1600 cm^{-1}). Experimental and theoretical intensities in L mol^{-1} cm^{-1}; frequencies in cm^{-1}.

experimental spectrum, while they clearly are in the calculated spectrum. The fundamentals 26/27 were not resolved in the experimental VCD and IR spectra, while they are separated in the calculated spectrum. The same can be said about fundamentals 31/32. Given the number of bands in the spectra, it is unsurprising that sometimes bands overlap in either the experimental or theoretical spectrum.

More problematic than the band absorption frequencies are the intensities of transitions. These significant differences between theory and experiment are often found.[37] The intensity of fundamental 39/40 seems to be overestimated in the calculated IR spectrum. In the theoretical spectrum the intensity of fundamental 36 is overestimated, since the band is not visible in the experimental VCD spectrum. Fundamentals 23/24 are not clearly visible in the experimental VCD spectrum.

The band visible at 1520 cm^{-1} in the IR spectrum cannot be explained by the calculations and is probably due to impurities in the solvent during the measurements.

More important than the intensities and individual resolution of the peaks is that the signs of the fundamentals are

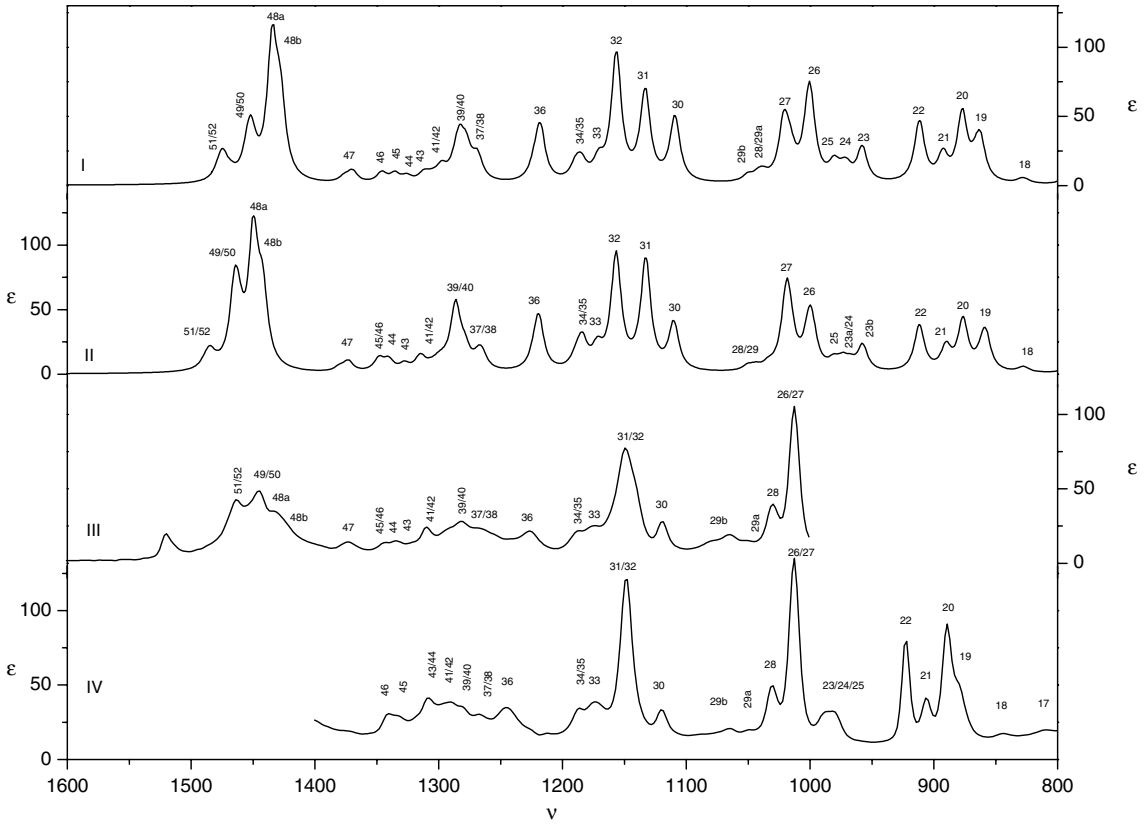

Figure 6. Assignment of the bands. B3LYP/6-31G* (II) and B3LYP/cc-pVTZ (I) simulated IR spectra for (1*R*,2*S*,5*R*,6*S*)-**1**. Experimental IR spectrum in CS_2 (III) and $CDCl_3$ (IV) of (+)-**1**. Experimental and theoretical intensities in L mol^{-1} cm^{-1}; frequencies in cm^{-1}.

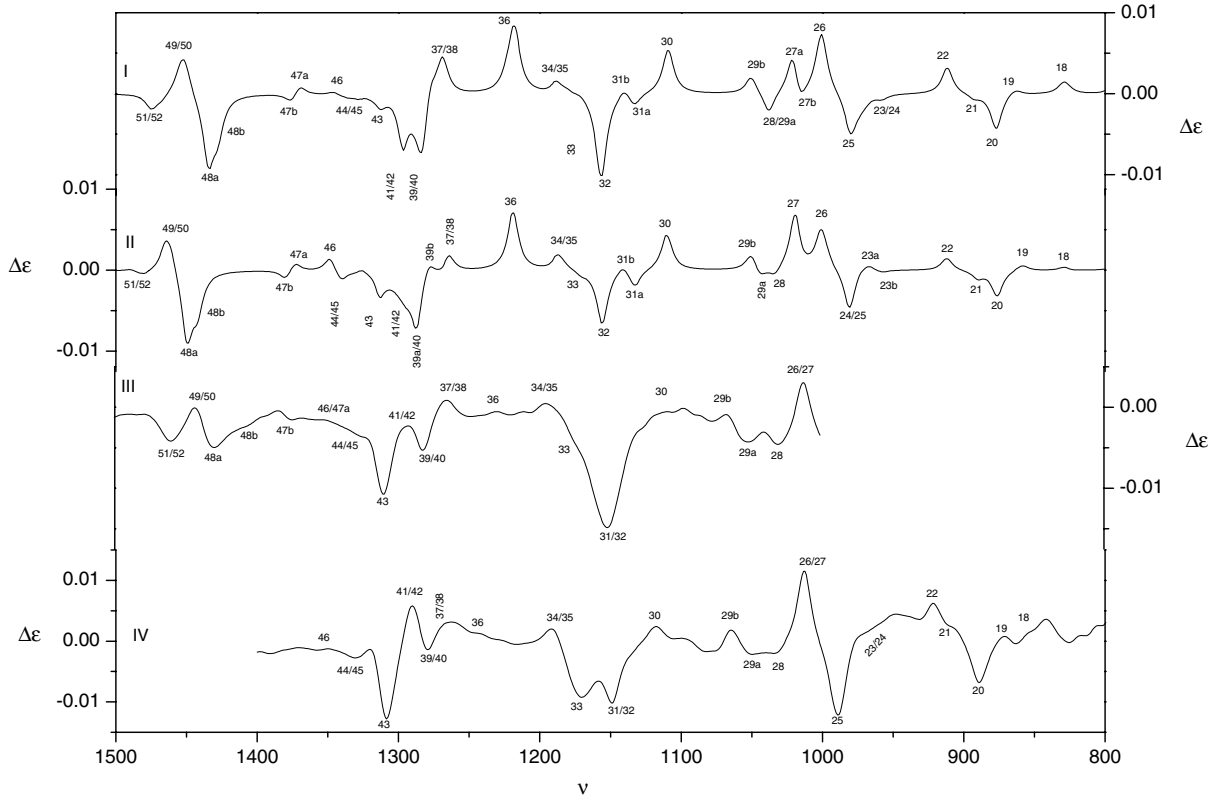

Figure 7. Assignment of the bands. B3LYP/6-31G* (II) and B3LYP/cc-pVTZ (I) simulated VCD spectra for (1*R*,2*S*,5*R*,6*S*)-**1**. Experimental VCD spectrum in CS_2 (III) and $CDCl_3$ (IV) of (+)-**1**. Experimental and theoretical intensities in L mol^{-1} cm^{-1}; frequencies in cm^{-1}.

mostly predicted correctly. The study of the agreement of spectra is, in first instance, based on this agreement. However, even then, small differences can appear. Fundamentals 41/42 in the VCD spectrum, measured in CS_2, have a positive sign while they are predicted to be negative. Correlation coefficients of 0.73 and 0.52 were obtained for the dipole and rotational strengths, respectively. It is well known that for VCD these values are quite often relatively low, especially for larger molecules. As such, these quantitative comparisons are not decisive.

The cc-pVTZ spectra, also shown in Figures 6 and 7, agree very well with the 6-31G* spectra.

Given the good agreement between the experimental and theoretical (1*R*,2*S*,5*R*,6*S*)-**1** spectra and the lack of any good agreement with the other diastereomers, the absolute configuration of (+)-**1** was concluded to be (1*R*,2*S*,5*R*,6*S*)-**1**.

For each possible configuration of **2**, the Boltzmann weighted IR and VCD spectra have been constructed. In Figures 8 and 9, the calculated spectra were compared to the experimental IR and VCD spectrum, respectively. Taking into account the IR spectra only, no conclusion could be made about the discrimination of the diastereomers. The signs of two patterns in the VCD spectrum give extra information for the assignment. In the calculated spectra of the second (*SRSS*) and third (*SRSR*) configuration, an intense positive band is immediately followed by a large negative one in the region between 1200 and 1300 cm^{-1}. This is in agreement with the experimental band signs in that

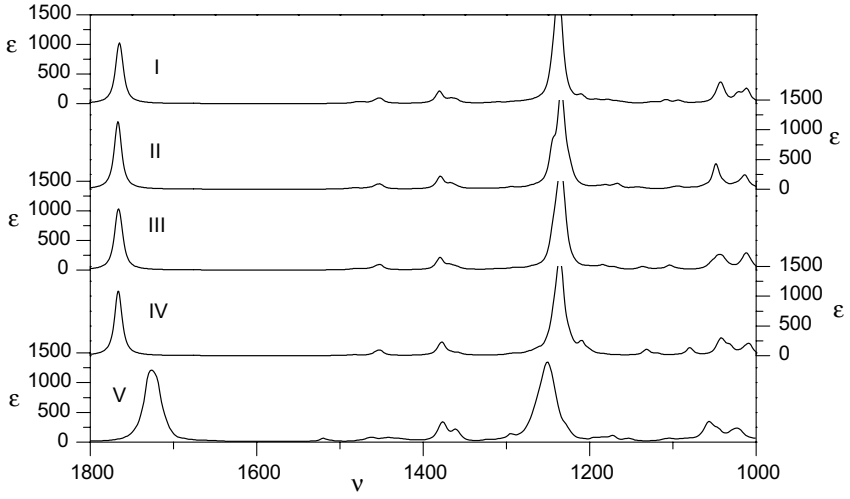

Figure 8. B3LYP/6-31G* IR spectra of each diastereomer of **2**: I—*SSSS*, II—*SRSR*, III—*SRSS* and IV—*RRSR*. Experimental unpolarized IR absorption spectrum of (+)-**2** (V) in $CDCl_3$ (1000–1600 cm^{-1}). Experimental and theoretical intensities in L mol^{-1} cm^{-1}; frequencies in cm^{-1}.

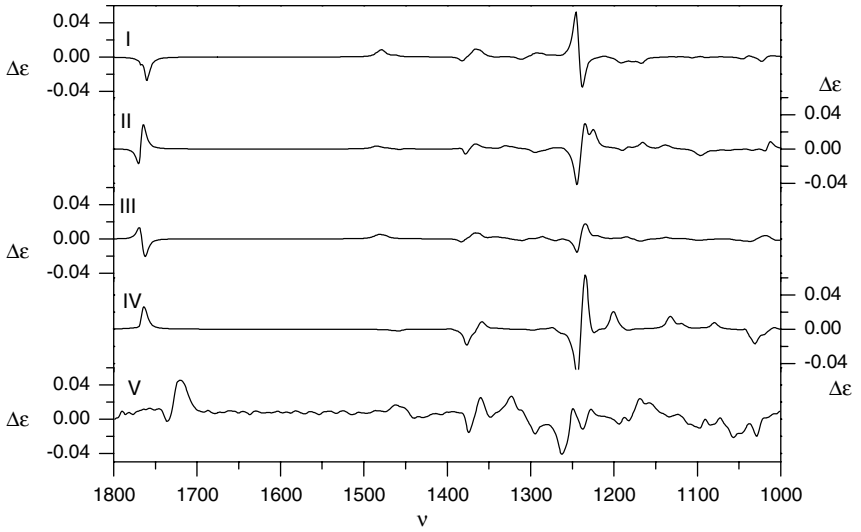

Figure 9. B3LYP/6-31G* VCD spectra of each diastereomer of **2**: I—*SSSS*, II—*SRSR*, III—*SRSS* and IV—*RRSR*. Experimental VCD absorption spectrum of (+)-**2** (V) in $CDCl_3$ (1000–1600 cm^{-1}). Experimental and theoretical intensities in L mol^{-1} cm^{-1}; frequencies in cm^{-1}.

region. The opposite patterns were found in the calculated spectra of the first (*RRSR*) and the last (*SSSS*) configurations, which could suggest their corresponding enantiomers. A second pattern, however, leads to the exclusion of three of the configurations. The VCD pattern of the CO stretching vibration (1700–1800 cm^{-1}) in the experimental spectrum gave rise to an intense positive band, followed by an intense negative band. The corresponding patterns in the calculated VCD spectra of configurations *RRSR* and *SSSS* are totally different from the experiment. Only one positive, respectively, negative band is visible. In configuration *SRSS* two bands are visible, but opposite in sign compared to the experiment. Only in the *SRSR* spectrum, the signs of the two patterns described above are in good agreement with the experiment. This immediately suggests the absolute configuration.

In order to be certain about the determination of the absolute configuration of (+)-**2**, each band in the experimental spectrum has to be linked with a band of the B3LYP/6-31G* spectrum of the *SRSR* configuration. The assignment is shown in Figures 10 and 11. There is a good overall agreement between the calculated and experimental IR spectra of **2**. Due to the large number of conformations that need to be taken into account, the assignment becomes more complex, especially in the region 1300–1500 cm^{-1}, the bands are not resolved. This, however, is in agreement with the experiment. Most of the bands in the experimental spectra cannot be attributed to a certain conformation, since their normal modes appear to have nearly identical frequencies. Two bands, however, around 1080 cm^{-1} can only be linked to a conformer with higher energy, and are labelled as *d*. The band visible at 1520 cm^{-1} is probably due to impurities in the solvent during the measurements. There is an overall agreement between the calculated and the experimental VCD spectrum of **2**. Again normal modes 46 and 47 originating from the conformer, *d*, are visible. In the VCD spectrum, the signs resolve some bands. This is especially the case for fundamentals 53/54/55 and 77/78. Still not all modes can be separated by looking at the VCD spectrum. Since the normal mode 51, originating from the minima, labelled by *a* and *c*, gives rise to a positive band and the same mode of the conformers, designated as *b* and *d*, leads to a negative band, two separate bands are visible in the VCD spectrum. The conformations, connected with those labels, are described in Table 2. The experimental dipole and rotational strengths have been linked to the calculated values. The correlation factors are 0.84 and 0.50 for the IR and VCD spectra, respectively.

For the cc-pVTZ spectra, small differences can be observed compared to the 6-31G* spectrum. The relative intensities of the normal modes 65/66 and 67/68 are different. In the VCD spectra, a few differences are also visible. None of

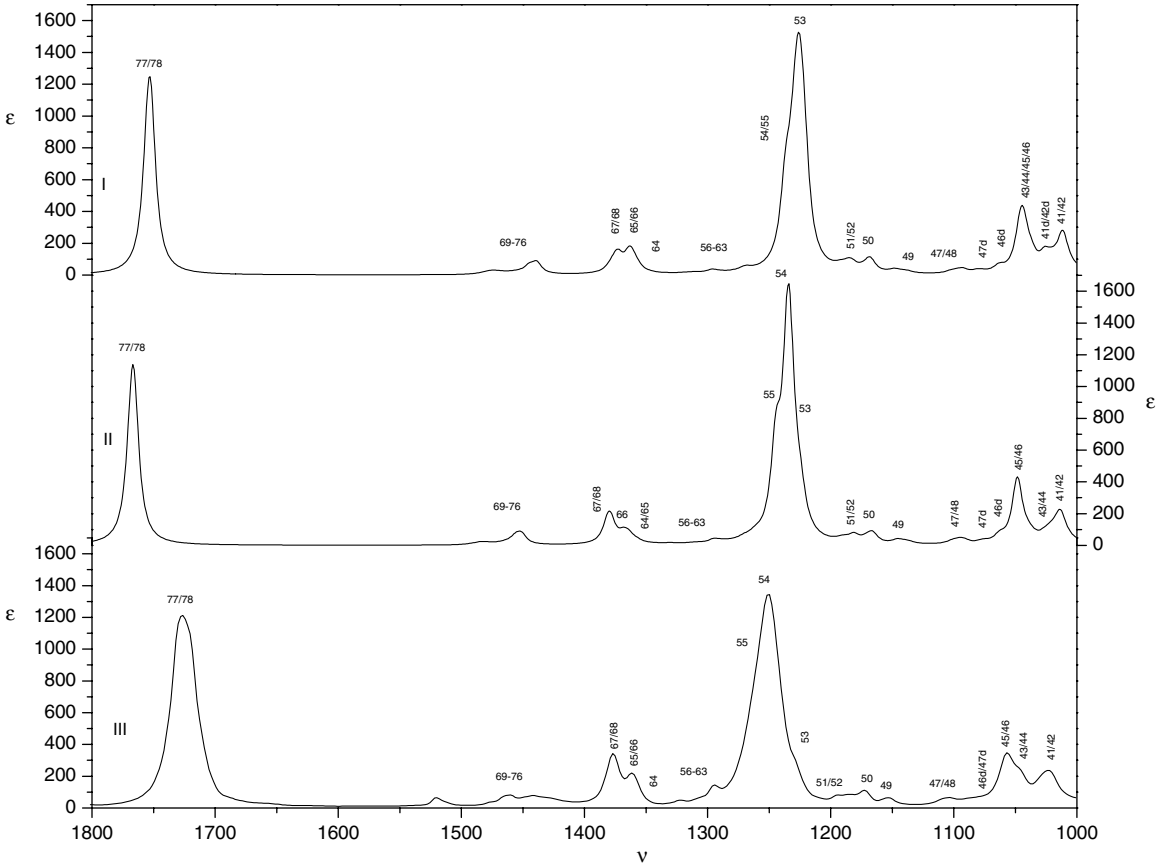

Figure 10. Assignment of the bands. B3LYP/6-31G* (II) and B3LYP/cc-pVTZ (I) simulated IR spectra for (1*S*,2*R*,5*S*,6*R*)-**2**. Experimental IR spectrum in $CDCl_3$ of (+)-**2** (III). Experimental and theoretical intensities L mol^{-1} cm^{-1}; frequencies in cm^{-1}.

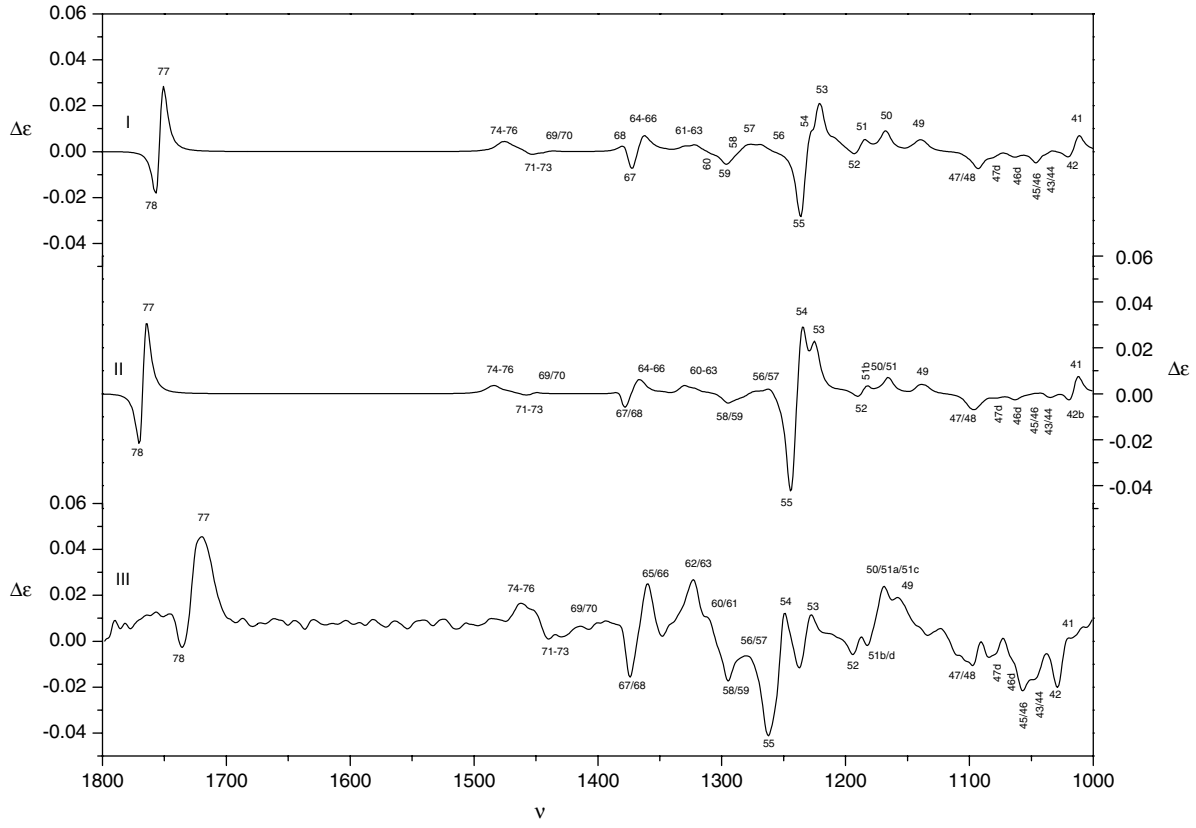

Figure 11. Assignment of the bands. B3LYP/6-31G* (II) and B3LYP/cc-pVTZ (I) simulated VCD spectra for (1*S*,2*R*,5*S*,6*R*)-**2**. Experimental VCD spectrum in $CDCl_3$ of (+)-**2** (III). Experimental and theoretical intensities in L mol^{-1} cm^{-1}; frequencies in cm^{-1}.

them, however, lead to a different assignment of the bands. The band originating from normal modes 45 and 46 is more important at the cc-pVTZ level. This trend is in better agreement with the experiment. At the cc-pVTZ level, the intensity of fundamental 54 is lower than fundamental 53. This is opposite to the 6-31G* calculations and the experiment. The 6-31G* basis set seems to be sufficient enough to determine that the absolute configuration of (+)-**2** corresponds to (1*S*,2*R*,5*S*,6*R*)-**2**.

This application of VCD for the determination of the absolute configuration illustrates how not only a good agreement between experiment and theory for one diastereomer is important, but also how the absolute configuration can be established by demonstrating that all other diastereomers give a much poorer agreement between theory and experiment.

The spectra of (1*R*,5*R*)-**3** have been calculated at the B3LYP/6-31G* level and were compared with the corresponding experimental spectra of (−)-**3**. There is an overall agreement between both spectra. The assignment of the experimental bands is shown in Figures 12 and 13. Label *a* corresponds to the conformer, with the lowest energy. Bands designated as *b* originate from the minimum, with the highest energy. Some differences were observed between the experimental and calculated IR spectra of **3**. In the experimental spectra fundamentals 26*a* and 26*b* were resolved, while they form one band in the B3LYP/6-31G* spectra. On the other hand fundamental 27 is not visible in experimental IR spectrum, while it clearly is in the calculated spectrum. Fundamental 34 is underestimated in the predicted spectrum. The intensity of band 28 is larger than band 26 in the experimental spectrum; this is opposite to the calculations. The agreement between the VCD spectra of **3** is excellent: all signs are predicted correctly. This has been confirmed by comparing the calculated and experimental dipole and rotational strengths of each band. Correlation factors of 0.89 and 0.67 have been obtained for the dipole and rotational strengths, respectively.

The cc-pVTZ and 6-31G* spectra show no large differences. The B3LYP/6-31G* level is sufficient to correctly assign the bands of the experimental spectra. It can be concluded that (1*R*,5*R*)-**3** corresponds to (−)-**3**.

The predicted spectra of (1*R*,5*R*)-**4** configuration have been constructed and compared to the experimental spectra of (−)-**4**. Frequencies and intensities have been calculated at the B3LYP/6-31G* level. In Figures 14 and 15, the assignment of each band in the experimental spectra is shown. The corresponding normal modes of all significant conformations are found to coincide. Looking at the most intense peaks, the best agreement occurs for the computed (1*R*,5*R*)-**4** absolute configuration. Molecule **4** is a good illustration of the fact that for larger molecules, more detailed features

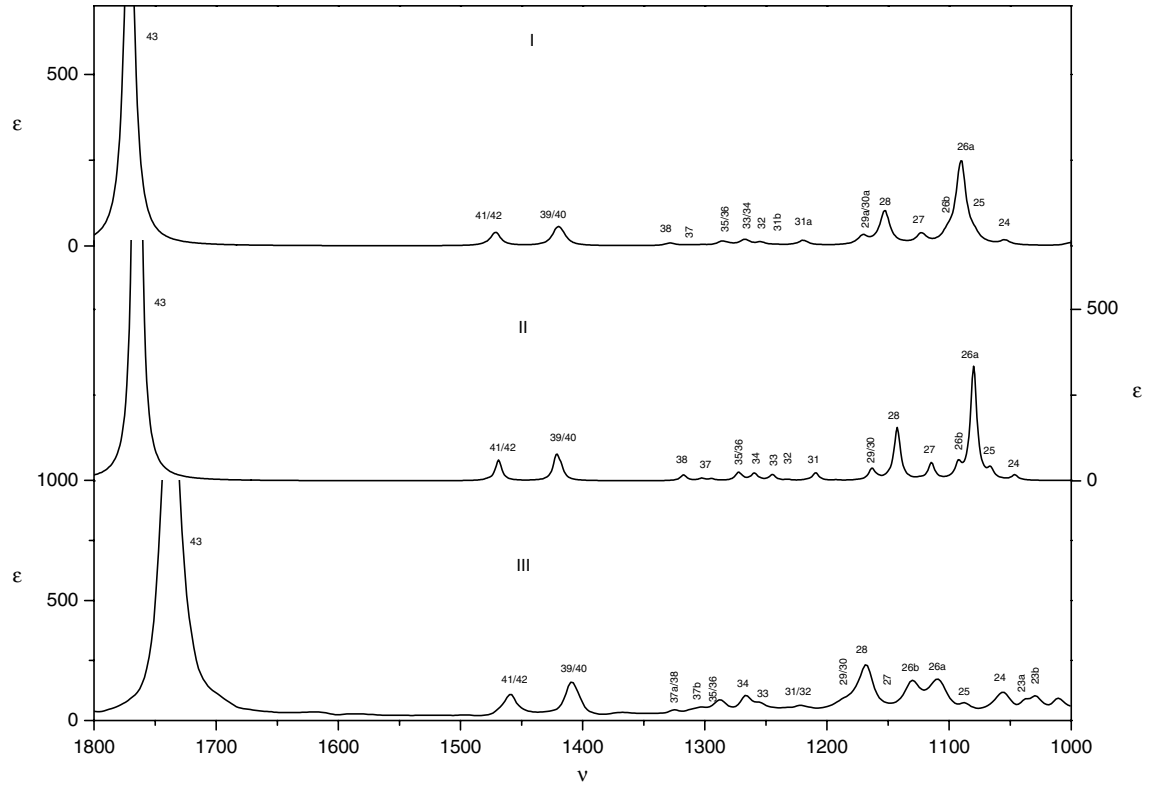

Figure 12. Assignment of the bands. B3LYP/6-31G* (II) and B3LYP/cc-pVTZ (I) simulated IR spectra for (1*R*,5*R*)-**3**. Experimental IR spectrum in $CDCl_3$ of (−)-**3** (III). Experimental and theoretical intensities in L mol^{-1} cm^{-1}; frequencies in cm^{-1}.

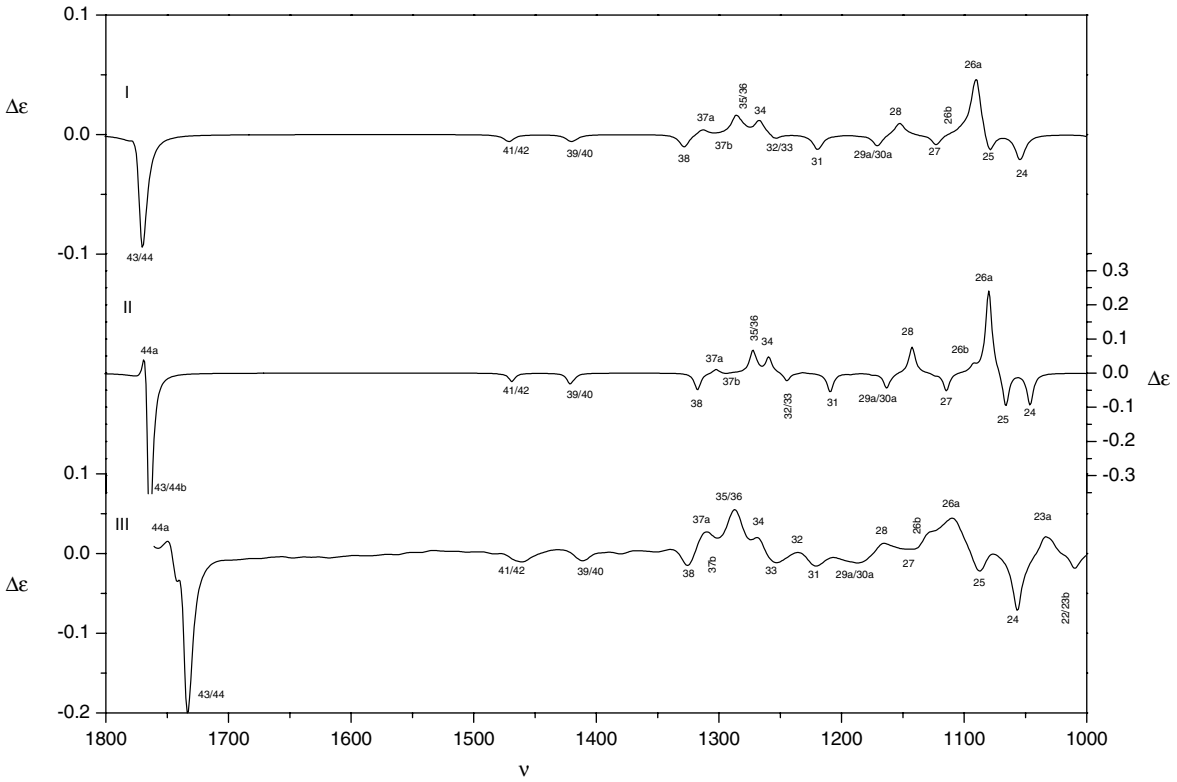

Figure 13. Assignment of the bands. B3LYP/6-31G* (II) and B3LYP/cc-pVTZ (I) simulated VCD spectra for (1*R*,5*R*)-**3**. Experimental VCD spectrum in $CDCl_3$ of (−)-**3** (III). Experimental and theoretical intensities in L mol^{-1} cm^{-1}; frequencies in cm^{-1}.

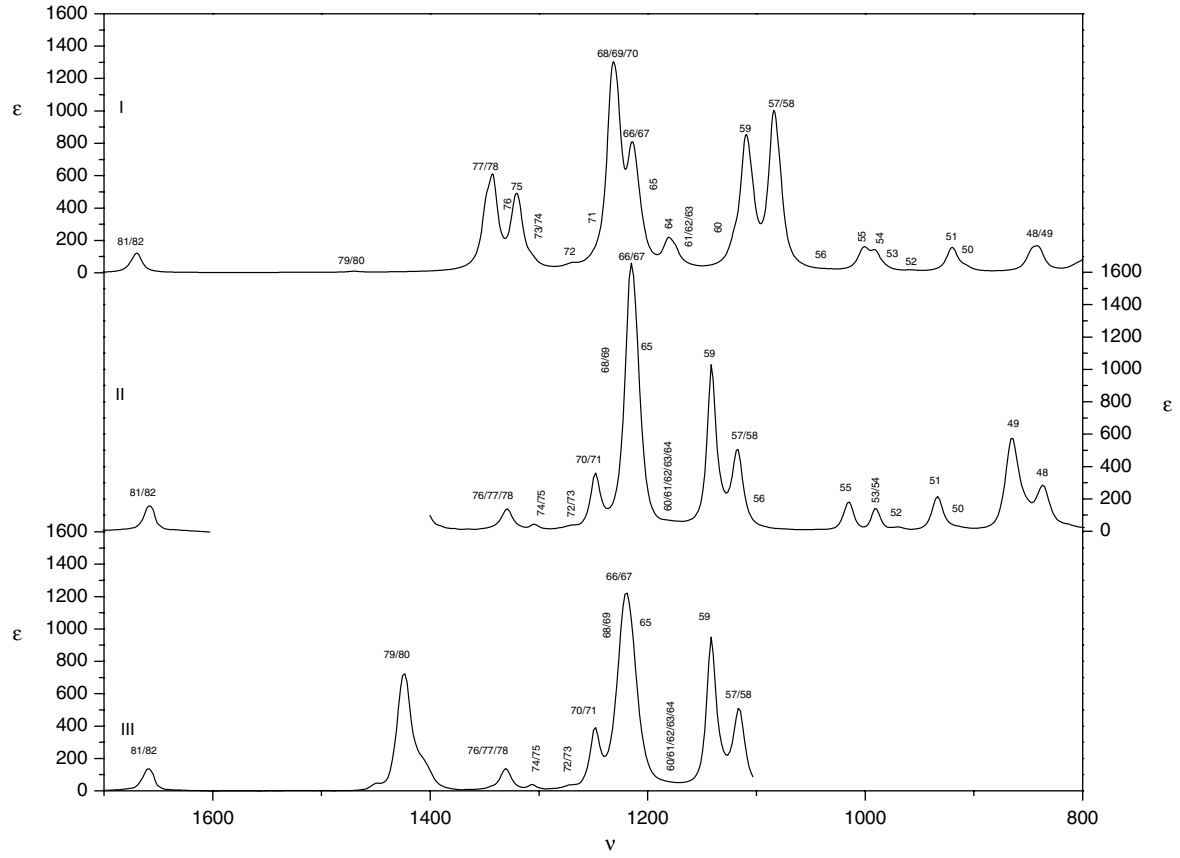

Figure 14. Assignment of the bands. B3LYP/6-31G* (I) simulated IR spectrum for (1*R*,5*R*)-**4**. Experimental IR spectra in CS_2 (II) and $CDCl_3$ (III) of (−)-**4**. Experimental and theoretical intensities in L mol^{-1} cm^{-1}; frequencies in cm^{-1}.

of the spectra may disagree between theory and experiment. This shows us that we must focus on the most intense peaks. Again, several bands are not well resolved, although the sign dimension in VCD does allow us to improve on the IR assignment. Coherent with the discussion above, relative intensities are also problematic for several peaks. All this shows that it is not evident to interpret the experimental VCD spectrum because of the small signal-to-noise ratio, especially in the frequency regions 1000–1100 and 120–1300 cm^{-1}. The signs of the most intense bands however were predicted correctly. Based on the most intense bands in both the experimental and the calculated VCD spectrum, it can be said that (−)-**4** corresponds to (1*R*,5*R*)-**4**. Correlation factors of 0.72 and 0.55 have been obtained for the IR and VCD spectra, respectively. Such values are quite typical for VCD based assignments of absolute configuration. The increase in the number of problems one is confronted with for molecules of increasing size is quite typical. This also explains why the application of VCD is most interesting when it is used as early as possible in a synthesis route as then often the molecules are still smaller. We have recently shown how the implementation of VCD as a part of the synthesis strategy can help establish the absolute configuration of the end product, which was far too large for VCD assignment. Naturally, this may require a re-thinking of the synthetic route as we must be absolutely sure that no change in the absolute configuration of racemization could occur in later stages.[38]

3. Conclusion

Using theoretical predictions based upon B3LYP/6-31G* and B3LYP/cc-pVTZ calculations, the absolute configurations of (+)-**1**, (+)-**2** and (−)-**3** were determined, respectively, as (1*R*,2*S*,5*R*,6*S*)-**1**, (1*S*,2*R*,5*S*,6*R*)-**2** and (1*R*,5*R*)-**3**. From the VCD study it can be concluded that (1*R*,5*R*)-**4** corresponds to (−)-**4**. For each molecule, the 6-31G* basis set appeared to be sufficient enough to allow the assignment. Moreover, no large differences were observed with respect to the cc-pVTZ calculations.

As expected by the chemical interconversions, the absolute configurations of (+)-**1**, (−)-**3** and (−)-**4** are the same, that is, (1*R*,5*R*)-stereochemistry. The absolute configuration of (+)-**2** is opposite.[4,13]

It has been shown that the VCD technique is very useful for the determination of absolute configuration, even when several diastereomers are possible.

4. Experimental

4.1. General

Reagents were purchased and used without purification. Lipase PS (*P. cepacia*) was obtained from Amano Enzyme

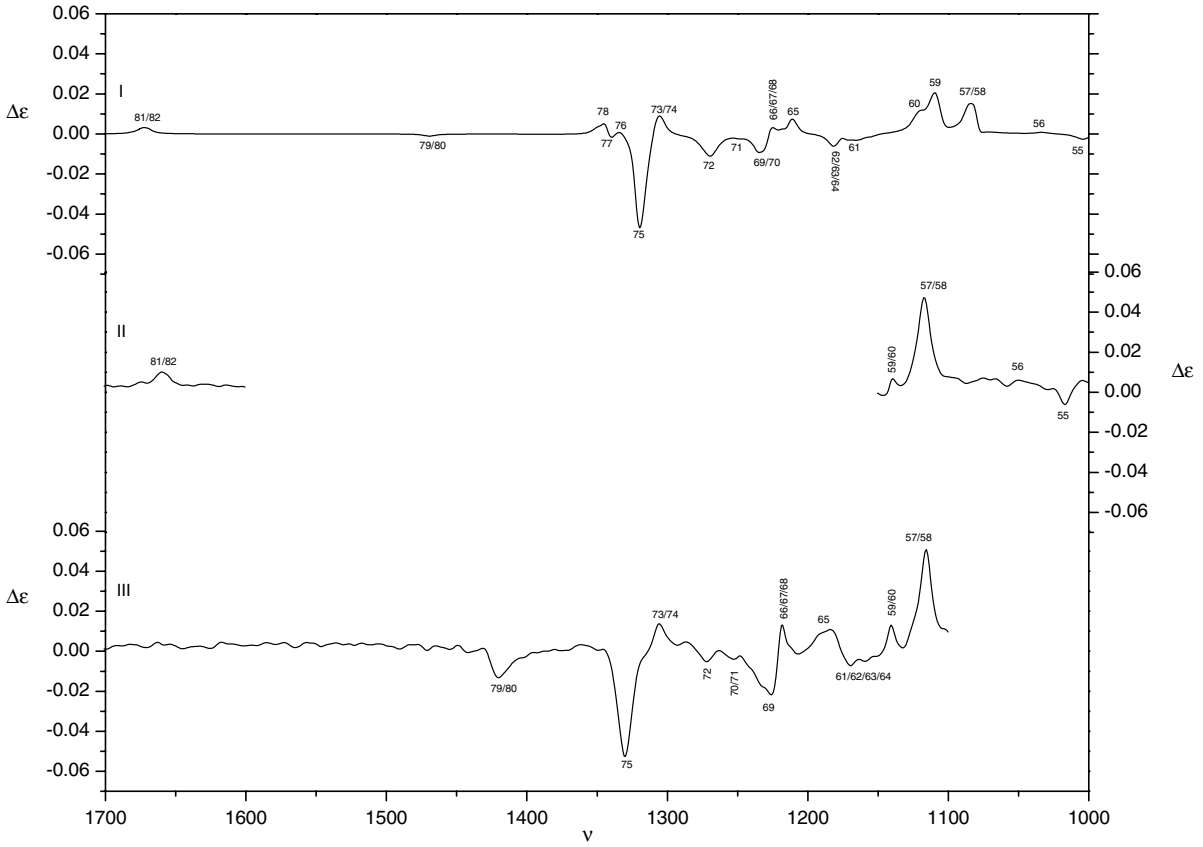

Figure 15. Assignment of the bands. B3LYP/6-31G* (I) simulated VCD spectrum for (1*R*,5*R*)-**4**. Experimental VCD spectra in CS_2 (II) and in $CDCl_3$ (III) of (−)-**4**. Experimental and theoretical intensities in L mol^{-1} cm^{-1}; frequencies in cm^{-1}.

Europe. The indicated R_f-values are for Macherey-Nagel SIL UV254 TLC-plates. Flash chromatography was carried out with Merck kieselgel 60, 30–75 μm or Merck silica gel 60F254. ^1H NMR and ^{13}C NMR spectra were recorded on a Bruker Avance 300 or a Bruker AM 500 spectrometer, with chemical shifts reported in parts per million relative to the residual solvent signal. IR-spectra are recorded with a Perkin–Elmer 160 FT-IR spectrometer. Optical rotations are determined with a Perkin–Elmer 241 polarimeter. Mass spectra were recorded with a Hewlett-Packard 5988A mass spectrometer. Chiral GC analysis was carried out on an Supelco Beta-Dex (30 m × 0.25 mm × 0.25 μm) column, Chiral HPLC analysis was carried out on a Chiralpak AD-H column. The resolution of (±)-**1** with lipase PS by a literature procedure,[1] resulted, beside (+)-(1*R*,2*S*,5*R*,6*S*)-**1** and (+)-(1*S*,2*R*,5*S*,6*R*)-**2** in 17% monoacetylated product ((+)-(1*S*,2*R*,5*S*,6*R*)-, 70–75% ee).[1] The reaction was monitored by GC: Alltech Econo-Cap Carbowax: 30 m × 0.32 mm × 0.25 μm: $T = 180$–200 °C (5 °C/min), **2**: 5.0 min, monoacetate: 5.7 min, **1**: 6.3 min. Data for the known compounds (+)-**1**, (+)-**2** and (−)-**3**.

4.1.1. (+)-(1*R*,2*S*,5*R*,6*S*)-1. Mp: 28–30 °C; $[\alpha]_D^{20} = +45.3$ (*c* 1.0, $CHCl_3$), $[\alpha]_{365}^{20} = +130.5$ (*c* 1.0, $CHCl_3$); {lit.: (1*R*,2*S*,5*R*,6*S*)-**1**: $[\alpha]_D^{20} = +44.0$ (*c* 2.122, $CHCl_3$, 90% ee),[11] $[\alpha]_D^{20} = +42.5$ (*c* 1.0, $CHCl_3$, 98.5%),[1] $[\alpha]_D^{27} = +49.5$ (*c* 2, $CHCl_3$, ee >99%)[3]} Chiralpak AD-H column, flow rate = 1 mL/min, $T = 35$ °C solvent: *n*-hexane/EtOH (90:10), retention time: (−)-(1*S*,2*R*,5*S*,6*R*)-**1** = 12.2 min, (+)-(1*R*,2*S*,5*R*,6*S*)-**1** = 14.2 min. GC: Supelco Beta-dex 120, $T = 160$ °C, t_R: (1*S*,2*R*,5*S*,6*R*)-(+)-**1** = 15.6 min, (−)-(1*R*,2*S*,5*R*,6*S*)-**1** = 15.9 min.

4.1.2. (+)-(1*S*,2*R*,5*S*,6*R*)-2. Mp: 37–39 °C (lit.: 37.5–39 °C[11]), $[\alpha]_D^{20} = +112.0$ (*c* 2.19, $CHCl_3$), $[\alpha]_{365}^{20} = +561.5$ (*c* 2.19, $CHCl_3$); {lit.: (1*S*,2*R*,5*S*,6*R*)-**2**: $[\alpha]_D^{20} = +113.1$ (*c* 2.065, $CHCl_3$, ee >99%)[11] $[\alpha]_D^{20} = +104.3$ (*c* 1, $CHCl_3$, 96.5% ee);[1] $[\alpha]_D^{26} = +115.0$ (*c* 2.26, $CHCl_3$, ee >99%)[3]}; GC: Supelco Beta-dex 120, $T = 165$ °C, t_R: (−)-(1*R*,2*S*,5*R*,6*S*)-**2** = 13.1 min, (+)-(1*S*,2*R*,5*S*,6*R*)-**2** = 13.6 min.

4.1.3. (−)-(1*R*,5*R*)-3. Mp: 36 °C (lit.: 43 °C);[13] $[\alpha]_D^{20} = -398$ (*c* 0.25, EtOH), $[\alpha]_{365}^{20} = -2019$ (*c* 0.25, EtOH); lit.: (1*S*,5*S*)-**9.2**: $[\alpha]_D^{20} = +394$ (*c* 0.25, EtOH);[13] GC: Supelco Beta-dex 120, $T = 155$ °C, t_R: (−)-**9.2** = 8.2 min, (+)-**9.2** = 8.5 min.

4.2. Synthesis of (1*R*,5*R*)-(−)-4

To (−)-**3** (4.200 g, 138.16 g/mol, 30.40 mmol) in a flask (1 L) equipped with an addition funnel, dry THF (215 mL) was added. The solution was cooled to −78 °C. Via the addition funnel, KHMDS (0.5 M in toluene, 133.8 mL, 66.9 mmol, 2.2 equiv) was added dropwise to the reaction mixture in 15 min. The addition funnel was

cleaned with dry THF (5 mL), which was also added to the reaction mixture. The mixture was then further stirred for 65 min at −78 °C. A solution of $PhNTf_2$ (25.00 g, 357.25 g/mol, 70.0 mmol, 2.3 equiv) in dry THF (75 mL) at room temperature was next added through a double tipped needle. Dry THF (30 mL) was used to rinse. Addition of $PhNTf_2$ and rinsing was completed in 25 min. The reaction mixture was next stirred for 1 h and 30 min at −78 °C, then for 30 min in an icebath and then next poured into a NH_4Cl solution (400 mL) with pentane (750 mL). The water layer was extracted once more with pentane (500 mL) and the combined organic layers were washed with saturated $NaHCO_3$ solution (300 mL). After drying over $MgSO_4$ and filtration, the low boiling solvents (THF and pentane) were removed under reduced pressure (~10–15 mmHg). The crude mixture in the remaining toluene was filtrated on a silica gel column (300 mL silica, 230–400 mesh, pentane/ether 1–2%) to remove the polar products. After removal of the volatiles under reduced pressure, (−)-**4** with apolar impurities (±19 g) was purified further by silica gel chromatography (1200 mL, 60–230 mesh) first eluting with pentane/toluene 1–2% followed by pentane/Et_2O 96/4, hereby flushing (−)-**4** (containing 1–2% $PhNTf_2$) from the column. After removal of the solvent under reduced pressure, an oil was obtained. An equal volume of pentane was added and, after half an hour the product crystallized. Filtration and washing with cold pentane (−20 °C) followed by repetition of the procedure on the obtained filtrate (3 times more) yielded 8.938 g (−)-**4** (0.0222 mol, 73%) as colourless crystals.

R_f: 0.47 (*cyclo*-hexane/Et_2O 90/10); mp = 32 °C; $[\alpha]_D^{20} = -49.2$ (*c* 0.97, $CHCl_3$), $[\alpha]_{365}^{20} = -147.3$ (*c* 0.97, $CHCl_3$); ^1H NMR (500 MHz, $CDCl_3$): $\delta = 5.62–5.65$ (2H, m), 3.61–3.65 (2H, m), 2.67 (2H, dm, $J = 17.1$ Hz), 2.51 (2H, dm, $J = 17.1$ Hz) ppm. ^{13}C NMR (75 MHz, $CDCl_3$): $\delta = 149.0$ (C), 118.5 (C, q, $J = 320$ Hz), 115.3 (CH), 44.1 (CH), 30.3 (CH_2) ppm. MS (*m*/*z*, %): 149 (38), 269 ([M−OTf], 100), 402 (M^+, 25) IR (KBr, film): 3094, 2935, 2871, 1660, 1455, 1426, 1331, 1307, 1250, 1209, 1140, 1114, 1016, 991, 934, 870, 839, 762, 660 cm^{-1}.

4.3. IR/VCD spectroscopy

The VCD spectra were recorded on a Bruker IFS 66/S FTIR interferometer, coupled to a Bruker PMA37 VCD module.[39]

A demountable cell with KBr windows and a 105 μm spacer has been used for all samples except for (−)-**4**, dissolved in $CDCl_3$ for which a CaF_2-cell with a 100 μm spacer was used. The unpolarized IR absorbance spectra were recorded at a resolution of 4 cm^{-1} and the VCD spectra at a resolution of 6 cm^{-1}. A 1830 cm^{-1} long wavepass filter was used to improve the VCD S/N ratio. The collection time for the VCD spectrum was 90 min, using six blocks of 15 min.

Samples of (+)-**1** and (−)-**4** have been prepared in $CDCl_3$ and CS_2 at an approximate concentration of 0.3 and 0.1 M, respectively. The use of both solvents yields a broad spectral range, that is, 800–1800 cm^{-1}. The IR and VCD spectra of (+)-**2** and (−)-**3** have been recorded in $CDCl_3$ at approximate concentrations of 0.07 and 0.2 M, respectively.

To obtain an estimate of the baseline artefacts, the VCD spectra of the solvents have been recorded, in the same conditions as the sample.[21]

4.4. Computational methods

The VCD spectra are composed of the contributions of the different conformations. Therefore, it is important to find the geometries of the relevant conformations of the molecule. The conformational landscape was explored by molecular mechanics (MM) and density functional theory. Stochastic searches in the MM3[40] and MM4[41] force fields have been executed as well as systematic searches using the MMFF[42,43] force field. The geometries that were located by molecular mechanics were subsequently optimized at the B3LYP/6-31G* level. A systematic search at the B3LYP/6-31G* level was also performed. The key dihedral angles were varied in a 60° grid. After a bump check and taking into account the ring constraints,[44] only chemically feasible starting structures were minimized on the B3LYP/6-31G* level.

The frequencies, dipole, and rotational strengths for each B3LYP/6-31G* minimum on the potential energy surface are calculated. The obtained line spectra of each conformer are then broadened by using a Lorentzian band-shape with a FWHM of 10 cm^{-1}. In order to make a comparison with the experimental spectra possible, the spectrum of each minimum is combined in a Boltzmann weighted manner. The conformational populations are based on the free energies of each conformation. Enthalpies and free energies were obtained using statistical thermodynamics. Appropriate scaling factors have been used to correct for the harmonic approximation.[45–47] For the calculations with the 6-31G* basis set, a uniform scaling factor of 0.967 was used, while in case of the cc-pVTZ calculations a factor of 0.977 was used. These values agree with the values found in the literature.[45]

The DFT calculations were performed with Gaussian 03 revision B05.[48] The B3LYP functional has been used together with the basis sets 6-31G* and cc-pVTZ.

The experimental dipole and rotational strengths have been determined by Lorentzian deconvolution of, respectively, the experimental IR and the VCD spectrum.

Acknowledgement

K.V. and E.D. are Research Assistants of the Fund for Scientific Research-Flanders (Belgium) (F.W.O.-Vlaanderen).

References

1. Lemke, K.; Ballschuh, S.; Kunath, A.; Theil, F. *Tetrahedron: Asymmetry* **1997**, *8*, 2051–2055.

2. Mehta, G.; Srinivas, K. *Tetrahedron Lett.* **2002**, *42*, 3319–3321.
3. Mehta, G.; Srinivas, K. *Tetrahedron Lett.* **2001**, *41*, 2855–2857.
4. Dyadchenko, M. A.; Melnikova, V. I.; Pivnitskii, K. *Zh. Obshch. Khim.* **1986**, *56*, 2143–2156.
5. Dyadchenko, M. A.; Danilova, G. A.; Shpanig, I.; Shik, G.; Pivnitskii, K. K. *Zh. Org. Khim.* **1990**, *26*, 2536–2542.
6. Cramer, N.; Laschat, S.; Baro, A.; Schwalbe, H.; Richter, C. *Angew. Chem., Int. Ed.* **2005**, *44*, 820–822.
7. Zhong, Y. W.; Jiang, C. S.; Xu, M. H.; Lin, G. Q. *Tetrahedron* **2004**, *60*, 8861–8868.
8. Zhong, Y. W.; Lei, X. S.; Lin, G. Q. *Tetrahedron: Asymmetry* **2002**, *13*, 2251–2255.
9. Zhong, Y. W.; Tian, P.; Lin, G. Q. *Tetrahedron: Asymmetry* **2004**, *15*, 771–776.
10. Henry, P. M.; Davies, M.; Ferguson, G.; Phillips, S.; Restivo, R. *J. Chem. Soc., Chem. Commun.* **1974**, 112–113.
11. Dyadchenko, M. A.; Pivnitsky, K. K. *J. Chem. Soc., Perkin Trans. 1* **1989**, 2001–2002.
12. Hungerhoff, B.; Sonnenschein, H.; Theil, F. *J. Org. Chem.* **2002**, *67*, 1781–1785.
13. Pérard-Viret, J.; Rassat, A. *Tetrahedron: Asymmetry* **1994**, *5*, 1–4.
14. Quast, H.; Janiak, R. *Liebigs Ann. Chem.* **1991**, *12*, 1305–1308.
15. Moriarty, R. M.; Duncan, M. P.; Vaid, R. K.; Prakash, O. *Org. Synth.* **1990**, *68*, 175–181.
16. Hagedorn, A. A.; Farnum, D. G. *J. Org. Chem.* **1977**, *42*, 3765–3767.
17. Hodgson, D. M.; Cameron, I. D.; Christlieb, M.; Green, R.; Lee, G. P.; Robinson, L. A. *J. Chem. Soc., Perkin Trans. 1* **2001**, *18*, 2161–2174.
18. Horikawa, T.; Norimine, Y.; Tanaka, M.; Sakai, K.; Suemune, H. *Chem. Pharm. Bull.* **1998**, *46*, 17–21.
19. Stephens, P. J.; Ashvar, C. S.; Devlin, F. J.; Cheeseman, J. R.; Frisch, M. J. *J. Mol. Phys.* **1996**, *89*, 579–594.
20. Stephens, P. J.; Devlin, F. J.; Cheeseman, J. R.; Frisch, M. J. *J. Phys. Chem.* **1994**, *98*, 11623–11627.
21. Stephens, P. J. Vibrational Circular Dichroism Spectroscopy: A New Tool for the Stereochemical Characterization of Chiral Molecules. In *Computational Medicinal Chemistry for Drugs Discovery*; Bultinck, P., De Winter, H., Langenaeker, W., Tollenaere, J. P., Eds.; Marcel Dekker: New York, 2004; pp 699–725.
22. Flack, H. D.; Bernardinelli, G. *Acta Crystallogr., Sect. A* **1999**, *55*, 908–915.
23. Hoye, T. R.; Hamad, A. S. S.; Koltund, O.; Tennakoon, M. A. *Tetrahedron Lett.* **2000**, *41*, 2289–2298.
24. Novy, J.; Urbanova, M.; Volka, K. *J. Mol. Struct.* **2005**, *748*, 17–25.
25. Vandyck, K.; Matthys, B.; Van der Eycken, J. *Tetrahedron Lett.* **2005**, *46*, 75–78.
26. Cheeseman, J. R.; Frisch, M. J.; Devlin, F. J.; Stephens, P. J. *Chem. Phys. Lett.* **1996**, *252*, 211–220.
27. Devlin, F. J.; Stephens, P. J.; Cheeseman, J. R.; Frisch, M. J. *J. Phys. Chem. A* **1997**, *101*, 9912–9924.
28. Stephens, P. J. *J. Phys. Chem.* **1985**, *89*, 748–752.
29. Kuppens, T.; Vandyck, K.; Van der Eycken, J.; Herrebout, W.; van der Veken, B. J.; Bultinck, P. *J. Org. Chem.* **2005**, *70*, 9103–9114.
30. Kuppens, T.; Langenaeker, W.; Tollenaere, J. P.; Bultinck, P. *J. Phys. Chem. A* **2003**, *107*, 542–553.
31. Polavarapu, P. L.; Zhao, C. X.; Cholli, A. L.; Vernice, G. G. *J. Phys. Chem. B* **1999**, *103*, 6127–6132.
32. Devlin, F. J.; Stephens, P. J. *J. Am. Chem. Soc.* **1999**, *121*, 7413–7414.
33. Muñoz, M. A.; Muñoz, O.; Joseph-Nathan, P. *J. Nat. Prod.* **2006**.
34. Solladie-Cavallo, A.; Marsol, C.; Yaakoub, M.; Azyat, K.; Klein, A.; Roje, M.; Suteu, C.; Freedman, T. B.; Cao, X.; Nafie, L. A. *J. Org. Chem.* **2003**, *68*, 7308–7315.
35. Vandyck, K.; Matthys, B.; Willen, M.; Robeyns, K.; Van Meervelt, L.; Van der Eycken, J. *Org. Lett.* **2006**, *8*, 363–366.
36. Ritter, K. *Synthesis* **1993**, *8*, 735–762.
37. Miller, M. D.; Jensen, F.; Chapman, O. L.; Houk, K. N. *J. Phys. Chem.* **1989**, *93*, 4495–4502.
38. Kuppens, T.; Herrebout, W.; Van Der Veken, B.; Corens, D.; De Groot, A.; Doyon, J.; Van Lommen, G.; Bultinck, P. *Chirality* **2006**, *18*, 609–620.
39. Urbanova, M.; Setnicka, V.; Volka, K. *Chirality* **2000**, *12*, 199–203.
40. Allinger, N. L.; Yuh, Y. H.; Lii, J. H. *J. Am. Chem. Soc.* **1989**, *111*, 8551–8566.
41. Allinger, N. L.; Chen, K. S.; Lii, J. H. *J. Comput. Chem.* **1996**, *17*, 642–668.
42. Halgren, T. A. *J. Comput. Chem.* **1996**, *17*, 490.
43. Halgren, T. A. *J. Comput. Chem.* **1996**, *17*, 520.
44. Sadowski, J.; Schwab, C. H.; Gasteiger, J. 3D Structure Generation and Conformational Searching. In *Computational Medicinal Chemistry for Drugs Discovery*; Bultinck, P., De Winter, H., Langenaeker, W., Tollenaere, J. P., Eds.; Marcel Dekker: New York, 2004; pp 151–212.
45. Koch, W.; Holthausen, M. C. *A Chemist's Guide to Density Functional Theory*, 2nd ed.; Strauss Offsetdruck: Germany, 2002.
46. Halls, M. D.; Velkovski, J.; Schlegel, H. B. *Theor. Chem. Acc.* **2001**, *105*, 413–421.
47. Scott, A. P.; Radom, L. *J. Phys. Chem.* **1996**, *100*, 16502–16513.
48. Frisch, M. J.; Trucks, G. W.; Schlegel, H. B.; Scuseria, G. E.; Robb, M. A.; Cheeseman, J. R.; Montgomery, J. A., Jr.; Vreven, T.; Kudin, K. N.; Burant, J. C.; Millam, J. M.; Iyengar, S. S.; Tomasi, J.; Barone, V.; Mennucci, B.; Cossi, M.; Scalmani, G.; Rega, N.; Petersson, G. A.; Nakatsuji, H.; Hada, M.; Ehara, M.; Toyota, K.; Fukuda, R.; Hasegawa, J.; Ishida, M.; Nakajima, T.; Honda, Y.; Kitao, O.; Nakai, H.; Klene, M.; Li, X.; Knox, J. E.; Hratchian, H. P.; Cross, J. B.; Adamo, C.; Jaramillo, J.; Gomperts, R.; Stratmann, R. E.; Yazyev, O.; Austin, A. J.; Cammi, R.; Pomelli, C.; Ochterski, J. W.; Ayala, P. Y.; Morokuma, K.; Voth, G. A.; Salvador, P.; Dannenberg, J. J.; Zakrzewski, V. G.; Dapprich, S.; Daniels, A. D.; Strain, M. C.; Farkas, O.; Malick, D. K.; Rabuck, A. D.; Raghavachari, K.; Foresman, J. B.; Ortiz, J. V.; Cui, Q.; Baboul, A. G.; Clifford, S.; Cioslowski, J.; Stefanov, B. B.; Liu, G.; Liashenko, A.; Piskorz, P.; Komaromi, I.; Martin, R. L.; Fox, D. J.; Keith, T.; Al-Laham, M. A.; Peng, C. Y.; Nanayakkara, A.; Challacombe, M.; Gill, P. M. W.; Johnson, B.; Chen, W.; Wong, M. W.; Gonzalez, C.; Pople, J. A. *Gaussian 03, Revision B.05*; Gaussian: Pittsburgh, PA, 2003.